




# Fuzzy C-Means Approach Optimized using Raindrop Algorithm for Image Segmentation

Bindu Puthentharayil Vikraman<sup>1\*</sup>  and Jabeena Afthab<sup>2</sup>

<sup>1,2</sup> SENSE, Vellore Institute of Technology, Vellore, PIN. 632014, India

bindup2005@gmail.com, ajabeena@vit.ac.in

**Abstract.** Medical image segmentation is critical in advancing healthcare systems, notably disease finding and medication scheduling. Because of its simplicity and efficacy, fuzzy c-means-based clustering emerged as an efficient algorithm for lesion extraction. The downsides of FCM include its sensitivity to beginning values, quick descent on local minima, and noise exposure. This study proposes a raindrop optimization idea, a soft clustering-based medical image segmentation algorithm with a noise reduction mechanism. A hybrid filter is a smoothing filter to exclude any potential interference in the image. The procedure implemented in MATLAB software detects and extracts tumors from brain magnetic resonance images from the BraTS data set. A comparative study of the proposed method with some cluster-based segmentation techniques reveals that the suggested system performs significantly better than the current cluster-based segmentation methods.

**Keywords:** FCM, Fuzzy c-means, Raindrop algorithm, Image segmentation.

## 1 Introduction

The process of classifying regions of an image that have similar characteristics or attributes is called image segmentation. Images are segmented based on pixel color, histograms of directed gradients, Local Binary patterns, etc.[1]. Medical imaging, object detection, remote sensing, and a wide range of other fields can benefit from segmentation [2]. Segmentation is used in medical imaging for image presentation, attribute extraction, and image measurement, among other things. Image segmentation is essential for finding anomalies in anatomical regions, including the brain and lungs, tumor identification, blood cell classification, surgery simulations, coronary border detection in angiograms, microcalcification detection on mammograms, and more [3-6].

Various segmentation methods have already been built and used in multiple applications. Two approaches for segmenting images are discontinuity-based and similarity-based [1],[7-9]. The discontinuity-based technique detects the sudden changes in an image's intensity values. In the latter method, pixels of comparable intensity values get grouped to enable the segmentation. This approach starts with a collection of seed points in the region-growing strategy and pixels that have the matching magnitude as the seed point forms an area. The region-growing method expands regions according

to their resemblance and closeness [10-11]. The split and merge approach creates a more prominent section by dividing the original image into miniature images, combined with residual images with comparable features [1-2], [12,13].

The soft clustering approach known as fuzzy C-means (FCM) is centered on a primary region-growing method [14-16]. In this algorithm, one data point can belong to multiple clusters. As a result of its efficiency and ease of use, FCM has emerged among the most extensively used clustering methods. However, FCM has the drawbacks of being sensitive to preliminary values, local optimal solutions, and noise sensitivity [17].

Zotien et al. [18] presented an FCM clustering algorithm incorporating denoising for image segmentation. The Canny operator detected the delicate boundaries of the images. The performance of an FCM clustering algorithm is affected by possible noise in the acquired image and a fixed value of the fuzzifier. Mishro et al. [19] proposed a segmentation approach that replaces a fixed fuzzifier with an adaptive linguistic fuzzifier. Misclassification of the noisy pixels was reduced by introducing the spatial details in the membership. Bakhtyar et al. [3] presented a clustering strategy for extracting lesions from a medical image. Their study mentioned various imaging and clustering approaches. Dhanachandra et al. [20] discussed a PSO algorithm for image segmentation. Furthermore, the anti-noise capacity is improved by a noise diminution process based on the neighboring pixels. MRI and synthetic picture data are used to assess the algorithm's performance.

Zhou et al. [21] presented the UNet++ architecture for accurate and instance picture segmentation. This approach employed a group of U-nets of varying depths that shared a piece of an encoder and learned together under deep supervision. A trimming process increases the processing speed. Chen et al. [22] proposed TransUNet as a tool for image segmentation. The findings exhibit that the indicated approach acts superior by retrieving focused spatial evidence. Hesamian et al. [23] examined image segmentation methodologies and network structures and their pros and cons. Debesh Jha et al. [24] introduced ResUNet++, an improved ResUNet architecture for colonoscope image segmentation. The results show that ResUNet++ outperforms the ResUNet structure.

Kirillov et al. [25] presented a classical computer graphics method for image segmentation. They demonstrated a neural network-based rendering network model. An iterative subdivision technique involves executing point-based segmentation projections at modifiable selected places.

In the Rain Optimization Method (ROA), demonstrated by Moazzeni et al. [26] the particle behaves similarly to optimization based on a gradient approach and conventional single-point algorithms such as hill-climbing. When a droplet starts moving, it will follow its path until it encounters the slightest barrier. All droplets would go through the same scenario. When a droplet achieves the lowest radius, its radius slowly lowers, considerably boosting the accuracy of the answer.

Kaboli et al. [27] presented an optimization algorithm, compared its accomplishment to various heuristic search methods, and found that the results were equivalent.

A thorough examination of current approaches reveals that better segmentation can enhance lesion detection and diagnosis accuracy. So, we propose an FCM clustering algorithm optimized with ROA enhanced with noise reduction to extract lesions in MR images.

The remaining part of this paper is arranged as follows. The second section discusses the suggested method in detail. The implementation results are discussed in section 3, and the main conclusion is presented in Section 4, followed by references.

## 2 Proposed methodology

In medical research and related areas, digital imaging plays a crucial role. Image segmentation techniques help in accurate diagnosis and treatment schedules [28,29]. White matter, cerebrospinal fluid, and gray matter are the three components that make up healthy brain matter. The characteristics of lesions in the brain vary. This research extracts lesions from brain MR images using feature-based clustering. There are four main steps in the suggested strategy. The gathering of image data for the evaluation of the algorithm's performance is the initial step. The needed data is from the BraTS 2018 dataset. A variety of noise could be present in the acquired image, such as speckle noise. This noise removal occurs in the second stage, the preprocessing. This stage makes use of a hybrid filter. The next step is segmentation using soft clustering. The ROA algorithm enhances the FCM clustering's performance. The segmented lesion and the background images result from this clustering stage.

## 3 FCM clustering approach

There are two kinds of clustering algorithms: hard clustering and soft clustering. A single data point fits into only one cluster in hard clustering, whereas data points in soft clustering can belong to multiple groups. FCM is used to segment the lesion in the magnetic resonance image. FCM is a fuzzy clustering algorithm centered on probability. In FCM, one data point can potentially belong to many clusters in this technique [1], [30].

Let the dataset be of  $n$  input data points given as  $S = \{s_1, s_2, s_3, \dots, s_n\}$ . We divide this datapoint into  $P$  groups or clusters,  $P = \{P_1, P_2, P_3, \dots, P_q\}$ . The algorithm optimizes the objective function by manipulating the evaluation components.

The objective function is presented by Eq.(1).

$$J = \sum_{q=1}^c \sum_{r=1}^n U_{qr}^m D_{qr}^2 \quad (1)$$

where, 'm' indicates the fuzzy element,  $U_{qr}$  represents the degree of truth and  $D_{qr}$  indicates the distance from the  $r^{th}$  instance to  $q^{th}$  cluster centroid. This parameter is represented by the Eq. (2).

$$D_{qr} = \|S_q - C_r\| \quad (2)$$

the degree of truth,  $s_i$  in  $j^{th}$  group is specified by the Eq. (3).

$$U_{ij} = \frac{D_{qr}^{\frac{2}{1-m}}}{\sum_{k=1}^c D_{kr}^{\frac{2}{1-m}}}, q \in [1, C], r \in [1, n] \quad (3)$$

and the centroid of the cluster is given by the Eq. (4)

$$C_q = \frac{\sum_{r=1}^n U_{qr}^m S_r}{\sum_{j=1}^n U_{qr}^m}, q \in [1, C] \quad (4)$$

### 3.1 Rain optimization algorithm (ROA)

The ROA is stimulated by the natural behavior of raindrops dripping down a slope toward a valley [26]. Droplets dropped on a flat surface may be sucked up by the soil or vanish by evaporation, whereas droplets that fall on a gradient surface may travel downward and join with other droplets. The droplet formation depends on the soil property and earth topology. If the droplet size is enormous, the scenario will be different. Large droplets can quickly combine, resulting in flooding. As a result, parameter adjustment is crucial in the raindrop optimization process. The raindrop optimization algorithm creates an initial population at random on the first iteration. The drop's neighbor point positions are contrasted to its location before advancing towards the lowest neighbor value. The raindrop will continue to descend until it reaches the valley. Even if there are pools on the way to the valley, if all the drops are dribbling down from a higher to a lower position, the RFO algorithm allows them to continue their travel to the canyon [31]. Evaporation or absorption can diminish the radius of a raindrop, but it can also increase as it interacts with other raindrops. Every single droplet's length is chosen haphazardly from an adequate choice. An individual droplet examines its proximity in every iteration, which is determined by its size. If a single droplet is still not tied to another droplet, look for the final limit of the region it has covered. As each droplet solves a problem in n-dimensional space, it contains n variables. Because the droplet radius will establish these bounds, the lower and upper limits of variable one will be investigated first [32]. This is followed by testing two of variable two's end-points and continues until the last variable is assessed. At this point, the first droplet's cost alters by pushing it below. This is not the droplet's last action and will continue to diminish in the same direction as the cost function falls. Once the entire droplet has been through this process, each droplet's position and cost will be ascertained.

If the parameters of this algorithm are properly calibrated, it can find both global and local extremums.

The first iteration of the algorithm begins with the random generation of the initial population. Assume that the population size is  $s$ . Then, the drop figure  $D_n$  can be described as

$$D^n = [s_{n,1}, s_{n,2}, s_{n,3}, \dots, s_{n,v}], n \in \{1,2,3, \dots, s\} \quad (5)$$

where  $v$  indicates the variables used in the optimization process.

When two droplets of radius  $r_1$  and  $r_2$  are close enough to one another, they may form a bigger drip with radius  $R$  defined by Eq. (6).

$$R = (r_1^f + r_2^f)^{1/f} \quad (6)$$

in which  $f$  denotes each droplet's variable count.

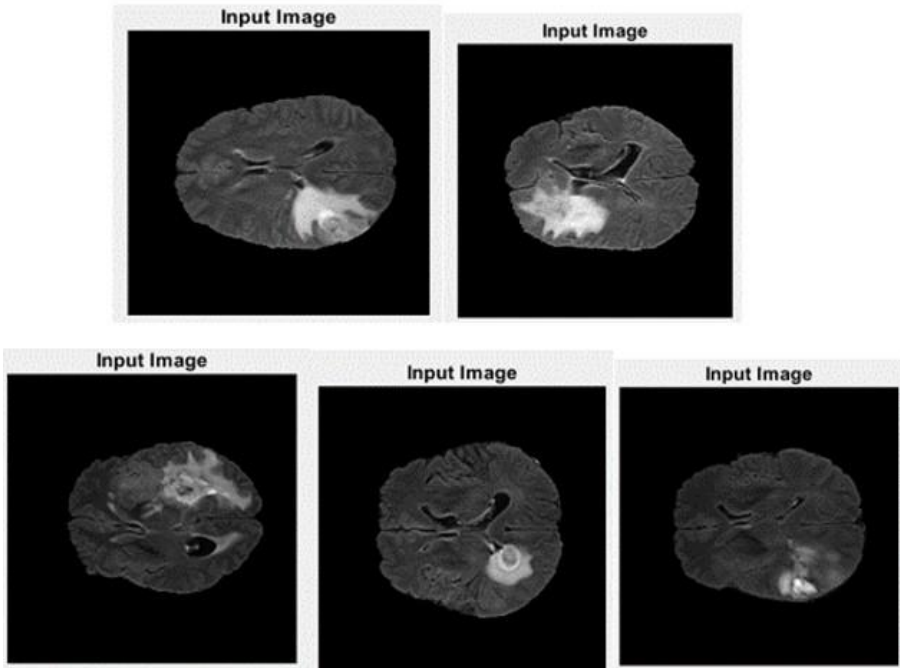
In the event when soil properties prevent a droplet from advancing, the radius can be given as in Eq. (7).

$$R = (\alpha r_1^f)^{1/f} \quad (7)$$

The population size decreases following a few repetitions, and larger dewdrops emerge. Increased iterations improve the speed with which effective solutions are identified, and the cluster group is created in the lowest amount of time while also reducing noise.

## 4 Results analysis

This segment examines the investigational outcomes achieved using the proposed method. MATLAB version 2021a is used to implement the offered plan. The public source BraTS 2018 provided the dataset used for the algorithm evaluation. The selected image has  $256 \times 256$ -pixel resolution. Figure 1 displays the pictures utilized in the evaluation of the algorithm. The input image, filtered image, and the segmented image for the selected five test images are shown in figure 2.

**Fig. 1.** Images used for lesion extraction

#### 4.1 Performance metrics

The metrics used for evaluation are the partition entropy (PE) and the partition coefficient (PC), which are defined below in Eq.(8) and (9).

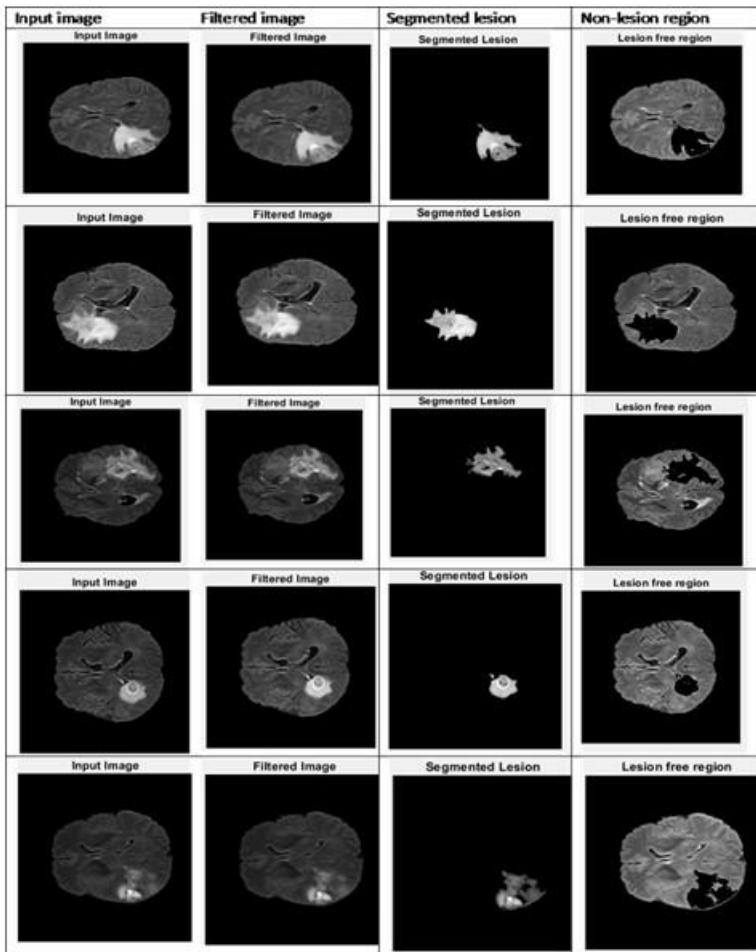
$$PC = \frac{\sum_i^N \sum_j^C U_{ij}^2}{N} \quad (8)$$

$$PE = \frac{\sum_i^N \sum_j^C U_{ij} \log U_{ij}}{N} \quad (9)$$

#### 4.2 Performance analysis

This segment presents the results obtained using the suggested algorithm. In Figure 2, the first column of images indicates the input images, and the second column shows the preprocessed, filtered images. The third and fourth columns indicate the

Fig. 2. Image output at different stages of the algorithm.



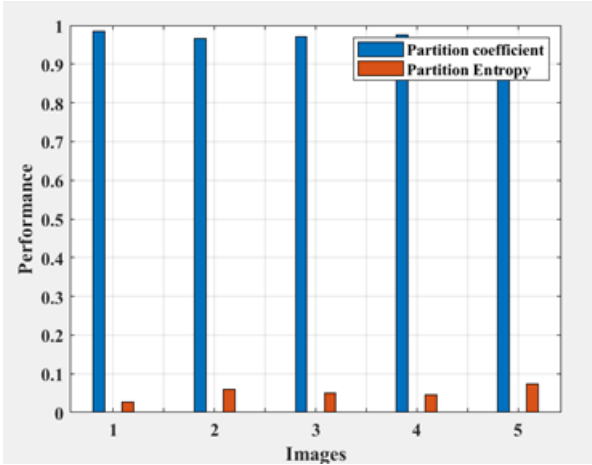
segmented lesion and non-lesion regions. Table 1 presents a performance comparison.

Table 1. Proposed Algorithm Outcomes

Sl.No.	PC	PE
1	0.9855	0.0265
2	0.9659	0.0597
3	0.9712	0.0508
4	0.9752	0.0447
5	0.9664	0.0544
Mean	0.9708	0.0472

of five medical images. The PC value for the examined data sets is 0.9708 on average, ranging from 0.9659 to 0.9855. The five selected pictures have an average PE value of

0.0472, ranging from 0.0265 to 0.0597. The comparison is depicted graphically in figure 3 below. The ideal clustering is achieved when PC and PE are at their maximum and minimal locations. PC and PE are in the  $[0,1]$  space. With a mean PC value of 0.9708, and a PE value of 0.0472, the suggested algorithm performs comparably.



**Fig. 3.** PC and PE comparison of selected images

The proposed algorithm is compared with Chaudhuri et al. [33], Dhanachandra et al. [20], and Chuang et al. [30] and is shown in table 2.

**Table 2.** Performance comparison

Technique applied	Partition coefficient (PC)	Partition entropy (PE)
IFPCM	0.7666	0.5766
DPSO-FCM	0.94	0.13
FCM-SFCM	0.888	0.234
Proposed method	0.9708	0.0472

The comparison is depicted graphically in figure 4 below. The proposed algorithm performs lesion detection with an average PC of 0.9708, and PE of 0.0472. The obtained PC value is better than the considered techniques. PE is better than all other techniques considered.



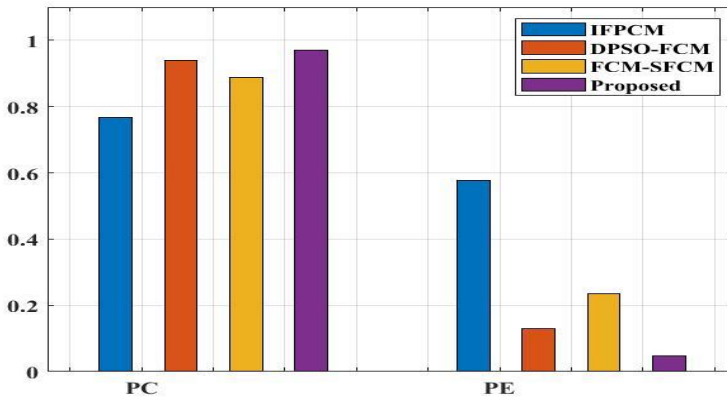


Fig. 4. Performance comparison

The outcome of the proposed system is appreciable compared to the existing methods.

## 5 Conclusion

This paper presented a competent tumor extraction strategy for medical images using a raindrop-optimized fuzzy c-means clustering algorithm. The public source BraTS 2018 provided the dataset for the algorithm performance assessment. A hybrid filter association is a mean, median, and Gaussian filter for noise reduction and smoothing operations. A comparative analysis of the proposed system for five medical images was performed. For the evaluated data sets, the PC value ranges from 0.9659 to 0.9855, and the PE varies from 0.0265 to 0.0597. A comparative study of the proposed method with some cluster-based segmentation techniques was conducted. The proposed algorithm performs lesion detection with an average PC of 0.9708 and PE of 0.0472. The outcome of the proposed system is appreciable compared to the existing cluster-based segmentation methods.

## References

1. P. K. Sran, S. Gupta, and S. Singh (2020), Segmentation based image compression of brain magnetic resonance images using visual saliency, *Biomed. Signal Process. Control*, vol. 62, p. 102089, 2020, doi: 10.1016/j.bspc.2020.102089.
2. Alireza Norouzi, Mohd Shafray Mohd Rahim, Ayman Altameem, Tanzila Saba, Abdolvahab Ehsani Rad, Amjad Rehman & Mueen Uddin (2014) *Medical Image Segmentation Methods, Algorithms, and Applications*, IETE Technical Review, 31:3, 199-213, DOI: 10.1080/02564602.2014.906861.
3. B. A. Mohammed and M. S. Al-ani,(2020), 'Digital Medical Image Segmentation Using Fuzzy C-Means Clustering,' vol. 4, no. 1, pp. 51–58, 2020, doi: 10.21928/uhdjst.v4n1y2020.pp51-58.

4. M. C. J. Christ and R. M. S. Parvathi, (2011) 'Fuzzy c-means algorithm for medical image segmentation,' ICECT 2011 - 2011 3rd Int. Conf. Electron. Comput. Technol., vol. 4, no. 1, pp. 33–36, 2011, doi: 10.1109/ICECTECH.2011.5941851.
5. R. U. Habib, "Optimal compression of medical images (2019)," *Int. J. Adv. Comput. Sci. Appl.*, vol. 10, no. 4, pp. 133–140, 2019, doi: 10.14569/ijacsa.2019.0100415.
6. SD. Kasute, M. Kolhekar, (2017). ROI Based Medical Image Compression. *International Journal of Scientific Research in Network Security and Communication*, 5(1), 6-11
7. P. Sreenivasulu and S. Varadarajan (2020), 'An Efficient Lossless ROI Image Compression Using Wavelet-Based Modified Region Growing Algorithm,' *J. Intell. Syst.*, vol. 29, no. 1, pp. 1063–1078, 2020, doi: 10.1515/jisys-2018-0180.
8. Y. Y. Chen(2007), "Medical image compression using DCT-based subband decomposition and modified SPIHT data organization," *Int. J. Med. Inform.*, vol. 76, no. 10, pp. 717–725, 2007, doi: 10.1016/j.ijmedinf.2006.07.002.
9. R. C. Gonzalez and R. E. Woods. "Digital Image Processing". 4th ed. Pearson Education, New York, 2018.
10. S. S. Parikh, D. Ruiz, H. Kalva, G. Fernandez-Escribano, and V. Adzic (2018), "High Bit-Depth Medical Image Compression with HEVC," *IEEE J. Biomed. Heal. Informatics*, vol. 22, no. 2, pp. 552–560, 2018, doi: 10.1109/JBHI.2017.2660482.
11. M. Singh, S. Kumar, S. Singh, and M. Shrivastava(2006), 'Various Image Compression Techniques: Lossy and Lossless,' *Int. J. Comput. Appl.*, vol. 142, no. 6, pp. 23–26, 2016, doi: 10.5120/ijca2016909829.
12. S. Saritha and N. Amutha Prabha (2016), "A comprehensive review: Segmentation of MRI images—brain tumor," *Int. J. Imaging Syst. Technol.*, vol. 26, no. 4, pp. 295–304, 2016, doi: 10.1002/ima.22201.
13. M. Revathi, R. Shenbagavalli, and T. Nadu,(2021) 'An efficient trapezoidal compression algorithm using wavelet transformation for medical image,' *J. Math. Comput. Sci.*, vol. 11, no. 5, pp. 5565–5579, 2021, doi: 10.28919/jmcs/6000.
14. Szilágyi, L., Benyó, Z., Szilágyi, S.M., & Adam, H. (2003). MR brain image segmentation using an enhanced fuzzy C-means algorithm. *Proceedings of the 25th Annual International Conference of the IEEE Engineering in Medicine and Biology Society (IEEE Cat. No.03CH37439)*, 1, 724-726 Vol.1.
15. Zhou, H., Schaefer, G., Shi, C. (2009). Fuzzy C-Means Techniques for Medical Image Segmentation. In: Jin, Y., Wang, L. (eds) *Fuzzy Systems in Bioinformatics and Computational Biology. Studies in Fuzziness and Soft Computing*, vol 242. Springer, Berlin, Heidelberg. [https://doi.org/10.1007/978-3-540-89968-6\\_13](https://doi.org/10.1007/978-3-540-89968-6_13).
16. B. P.V. and J. Afthab, (2021) 'Region of Interest Based Medical Image Compression Using DCT and Capsule Autoencoder for Telemedicine Applications,' 2021 Fourth International Conference on Electrical, Computer and Communication Technologies (ICECCT), Erode, India, 2021, pp. 1-7, doi: 10.1109/ICECCT52121.2021.9616748.
17. J. Horváth, "Image Segmentation Using Fuzzy C-Means." chrome-extension: //efaid-nbmnnibpcajpcglcfindmkaj/http://conf.uni-obuda.hu/sami2006/JurajHorvath.pdf", last accessed on 19th January 2023.
18. A. Zotin, (2018) 'ScienceDirect Edge detection in MRI brain tumor images based on fuzzy C-means clustering', *Procedia Comput. Sci.*, vol. 126, pp. 1261–1270, 2018, doi: 10.1016/j.procs.2018.08.069.
19. Mishro, P. K., Agrawal, S., Panda, R., & Abraham, A. (2020). A novel type-2 fuzzy C-means clustering for brain MR image segmentation. *IEEE Transactions on Cybernetics*, 51(8), 3901-3912.

20. Dhanachandra, N. and Chanu, Y.J., (2020). 'An image segmentation approach based on fuzzy c-means and dynamic particle swarm optimization algorithm'. *Multimedia tools and applications*, 79(25), pp.18839-18858.
21. Zhou, Z., Siddiquee, M. M., Tajbakhsh, N., & Liang, J. (2019). UNet++: Redesigning Skip Connections to Exploit Multiscale Features in Image Segmentation. *ArXiv*. <https://doi.org/10.48550/arXiv.1912.05074>
22. Chen, J., Lu, Y., Yu, Q., Luo, X., Adeli, E., Wang, Y., Lu, L., Yuille, A. L., & Zhou, Y. (2021). 'TransUNet: Transformers Make Strong Encoders for Medical Image Segmentation'. *ArXiv*. <https://doi.org/10.48550/arXiv.2102.04306>.
23. Hesamian, M.H., Jia, W., He, X. et al. (2019), 'Deep Learning Techniques for Medical Image Segmentation: Achievements and Challenges'. *J Digit Imaging* 32, 582–596 (2019). <https://doi.org/10.1007/s10278-019-00227-x>.
24. Jha, D., Smedsrud, P. H., Riegler, M. A., Johansen, D., de Lange, T., Halvorsen, P., & Johansen, H. D. (2019). ResUNet++: An Advanced Architecture for Medical Image Segmentation. *ArXiv*. <https://doi.org/10.48550/arXiv.1911.07067>.
25. Kirillov, A., Wu, Y., He, K., & Girshick, R. (2019). PointRend: Image Segmentation as Rendering. *ArXiv*. <https://doi.org/10.48550/arXiv.1912.08193>.
26. A. R. Moazzeni and E. Khamehchi, (2020) 'Rain optimization algorithm (ROA): A new metaheuristic method for drilling optimization solutions', *J. Pet. Sci. Eng.*, p. 107512, 2020, doi: 10.1016/j.petrol.2020.107512.
27. S. H. A. Kaboli, J. Selvaraj, and N. A. Rahim (2017), "Rain-fall optimization algorithm : a population based algorithm for solving constrained optimization problems," *J. Comput. Sci.*, (2017), doi: 10.1016/j.jocs.2016.12.010.
28. Minaee, S., Boykov, Y., Porikli, F., Plaza, A., Kehtarnavaz, N., & Terzopoulos, D. (2020). Image Segmentation Using Deep Learning: A Survey. *ArXiv*. <https://doi.org/10.48550/arXiv.2001.05566>
29. S. UmaMaheswari and V. SrinivasaRaghavan (2021), "Lossless mecal image compression algorithm using tetrolet transformation," *J. Ambient Intell. Humaniz. Comput.*, vol. 12, no. 3, pp. 4127–4135, 2021, doi: 10.1007/s12652-020-01792-8.
30. K. Chuang, H. Tzeng, S. Chen, J. Wu, and T. Chen (2006), "Fuzzy c-means clustering with spatial information for image segmentation," vol. 30, pp. 9–15, 2006, doi: 10.1016/j.comp-medimag.2005.10.001.
31. I. V Pustokhina, D. A. Pustokhin, P. T. Nguyen, M. Elhoseny, and K. Shankar (2021), "Multi-objective rain optimization algorithm with WELM model for customer churn prediction in telecommunication sector," *Complex Intell. Syst.*, 2021, doi: 10.1007/s40747-021-00353-6.
32. J. M. Guerrero-valadez, F. Martínez-rios, U. Panamericana, F. De Ingeniería, A. Rodin, and C. De México (2020), 'EAI Endorsed Transactions Rain-Fall Optimization Algorithm with new parallel implementations,' vol. 7, no. 29, pp. 1–13, 2020, doi: 10.4108/eai.13-7-2018.163981.
33. Arindam Chaudhuri, (2015) 'Intuitionistic Fuzzy Possibilistic C Means Clustering Algorithms', *Advances in Fuzzy Systems*, vol. 2015, Article ID 238237, 17 pages, 2015. <https://doi.org/10.1155/2015/238237>.

**Open Access** This chapter is licensed under the terms of the Creative Commons Attribution-NonCommercial 4.0 International License (<http://creativecommons.org/licenses/by-nc/4.0/>), which permits any noncommercial use, sharing, adaptation, distribution and reproduction in any medium or format, as long as you give appropriate credit to the original author(s) and the source, provide a link to the Creative Commons license and indicate if changes were made.

The images or other third party material in this chapter are included in the chapter's Creative Commons license, unless indicated otherwise in a credit line to the material. If material is not included in the chapter's Creative Commons license and your intended use is not permitted by statutory regulation or exceeds the permitted use, you will need to obtain permission directly from the copyright holder.

